J|A|C|S
ARTICLES
Published on Web 04/01/2003

Photoinduced Electron Transfer at Liquid|Liquid Interfaces: Dynamics of the Heterogeneous Photoreduction of Quinones by Self-Assembled Porphyrin Ion Pairs

Nicolas Eugster, David J. Fermín,* and Hubert H. Girault

Contribution from the Laboratoire d'Electrochimie Physique et Analytique, Institut de Chimie Moléculaire et Biologique, Ecole Polytechnique Fédérale de Lausanne, CH-1015 Lausanne, Switzerland

Received December 4, 2002; E-mail: david.fermin@epfl.ch

Abstract: The initial stages of the heterogeneous photoreduction of quinone species by self-assembled porphyrin ion pairs at the water|1,2-dichloroethane (DCE) interface have been studied by ultrafast time-resolved spectroscopy and dynamic photoelectrochemical measurements. Photoexcitation of the water-soluble ion pair formed by zinc *meso*-tetrakis(*p*-sulfonatophenyl)porphyrin ($ZnTPPS^{4-}$) and zinc *meso*-tetrakis(*N*-methylpyridyl)porphyrin ($ZnTMPyP^{4+}$) leads to a charge-separated state of the form $ZnTPPS^{3-}$–$ZnTMPyP^{3+}$ within 40 ps. This charge-separated state is involved in the heterogeneous electron injection to acceptors in the organic phase in the microsecond time scale. The heterogeneous electron transfer manifests itself as photocurrent responses under potentiostatic conditions. In the case of electron acceptors such as 1,4-benzoquinone (BQ), 2,6-dichloro-1,4-benzoquinone (DCBQ), and tetrachloro-1,4-benzoquinone (TCBQ), the photocurrent responses exhibit a strong decay due to back electron transfer to the oxidized porphyrin ion pair. Interfacial protonation of the radical semiquinone also contributes to the photocurrent relaxation in the millisecond time scale. The photocurrent responses are modeled by a series of linear elementary steps, allowing estimations of the flux of heterogeneous electron injection to the acceptor species. The rate of electron transfer was studied as a function of the thermodynamic driving force, confirming that the activation energy is controlled by the solvent reorganization energy. This analysis also suggests that the effective redox potential of BQ at the liquid|liquid boundary is shifted by 0.6 V toward positive potentials with respect to the value in bulk DCE. The change of the redox potential of BQ is associated with the formation of hydrogen bonds at the liquid|liquid boundary. The relevance of this approach toward modeling the initial processes in natural photosynthetic reaction centers is briefly discussed.

1. Introduction

Porphyrins and quinone species are key components in the initial stages of photosynthetic reactions in bacteria and green plants. For instance, the photosynthetic reaction center of *Rhodopseudomonas viridis* and *Rhodobacter sphaeroides* features four bacteriochlorophylls, two bacteriopheophytins, and two quinones organized in a pseudo-C_2 symmetry as depicted in Scheme 1.[1−3] Electron transfer from the photoexcited *special pair* to the pheophytin takes places within 4 ps.[4] The electron is subsequently transferred to the quinone Q_A in approximately 200 ps. The reaction proceeds via regeneration of the special pair by the cytochrome (20 ns) and electron transfer from Q_A to Q_B in 0.2 ms. The quinone Q_B is initially located at the interface between the plasmatic membrane and the cytosol, where it receives two electrons and two protons before diffusing to the cytochrome bc_1. Theoretical studies indicate that the transmembrane potential and the spatial distribution of the prostheic groups determined by the intrinsic proteins are

Scheme 1. Representation of the Photosynthetic Reaction Center of Purple Bacteria[a]

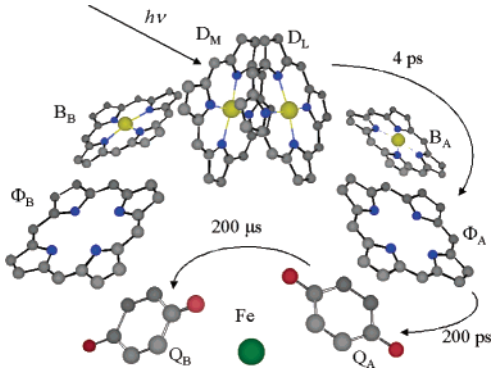

[a] D_M and D_L denote the bacteriochlorophyll molecules of the special pair and B_A and B_B denote accessory chlorophylls assisting the electron transfer to the bacteriopheophytins Φ_A and Φ_B, while Q_A and Q_B correspond to the ubiquinone molecules. The arrows indicate the electron pathway after the initial photon capture by the special pair. The phytyl chains of the bacteriochlorophylls and the side chain of the ubiquinones were omitted for clarity.

(1) Deisenhofer, J.; Epp, O.; Miki, K.; Huber, R.; Michel, H. *Nature* **1985**, 618.
(2) Chambron, J.-C.; Chardon-Noblat, S.; Harriman, A.; Heitz, V.; Sauvage, J.-P. *Pure Appl. Chem.* **1993**, *65*, 2343−2349.
(3) Hutter, M. C.; Hughes, J. M.; Reimers, J. R.; Hush, N. S. *J. Phys. Chem. B* **1999**, *103*, 4906−4915.
(4) Holzapfel, W.; Finkele, U.; Kaiser, W.; Oesterhelt, D.; Scheer, H.; Stilz, H. U.; Zinth, W. *Proc. Natl. Acad. Sci. U.S.A.* **1990**, *87*, 5168−5172.

10.1021/ja029589n CCC: $25.00

determinant factors in the efficiency of the photoreaction.[3,5] However, the design of artificial systems for studying the effect of the interfacial potential on the reactivity of model compounds remains a formidable challenge.

The dual role of quinones as redox relay and proton shuttle has been the subject of numerous electrochemical studies.[6−8] In aprotic solvents, quinones can be reversibly reduced to radical anions and dianions. However, protonation of the reduced quinones and formation of hydrogen bonds can introduce substantial changes in the effective redox potential depending on the nature of the functional groups in the quinone ring.[9−12] These are key phenomena in the reactivity of quinones at biological membranes. A relatively unexplored approach to the interfacial reactivity of quinones involves polarizable junctions between two immiscible electrolyte solutions.[13] At these interfaces, the kinetics of the heterogeneous reduction of quinones in the organic phase by hydrophilic redox species can be studied as a function of the Galvani potential difference. The appealing aspect of this approach is that the electron acceptor is confined in an aprotic media, yet it can interact with protons and form hydrogen bonds interfacially.

In this paper, we shall study the photoinduced reduction of a variety of quinone species by water-soluble porphyrins self-assembled at the water|1,2-dichloroethane (DCE) interface. The analysis will be extended from the initial stages of the photoexcitation of the ion-pair zinc *meso*-tetrakis(*p*-sulfonatophenyl)porphyrin (ZnTPPS) and zinc *meso*-tetrakis(*N*-methylpyridyl)porphyrin (ZnTMPyP) in the aqueous phase to the formation of the radical anion of the electron acceptor in the organic electrolyte. Under potentiostatic conditions, the photoinduced heterogeneous electron transfer involving water-soluble dyes and hydrophobic redox species manifests itself by photocurrent responses.[14−21] The combination of ultrafast time-resolved spectroscopy and dynamic photoelectrochemistry revealed that photoexcitation of the porphyrin ion pair leads to a charge-separated state within 40 ps, which can subsequently reduce quinones located in the adjacent phase or recombine in the microsecond time scale. Other processes such as back electron transfer from the quinone to the oxidized ion pair, as well as protonation of the quinone radical anion, take place within several milliseconds. Similarities between these photoreactions and the initial stages of photosynthetic processes in purple bacteria are briefly discussed.

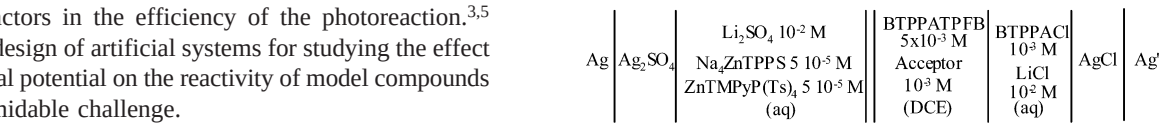

Figure 1. Schematic representation of the electrochemical cell employed for the photocurrent measurements. The abbreviation Ts stands for the tosylate anion.

2. Experimental Section

All reagents employed were analytical grade. The porphyrin salts $(Na)_4$ZnTPPS and ZnTMPyP(tosylate)$_4$ were purchased from Porphyrin Products, Inc. Bis(triphenylphosphoranylidene)ammonium tetrakis-(pentafluorophenyl)borate (BTPPATPFB) and Li_2SO_4 were employed as the organic and aqueous phase supporting electrolyte, respectively. The preparation of BTPPATPFB has been reported elsewhere.[18] Measurements were carried out in a three-compartment glass cell provided with two platinum counter electrodes and two luggin capillaries for the reference electrodes. The geometrical surface area was 1.53 cm^2. The electrochemical cell is represented in Figure 1. The water|1,2-dichloroethane (DCE) junction was polarized via a custom-built four-electrode potentiostat, and the potential scale was referred to formal transfer potential of the cation tetramethylammonium ($\Delta_o^w\phi^{o'}_{TMA^+} = 0.160$ V).[22] The liquid|liquid junction was illuminated with the 477 nm line of an Omnichrome S43 tuneable Ar-ion laser.

The redox potentials of tetracyanoquinodimethane (TCNQ), 1,4-benzoquinone (BQ), 2,6-dichloro-1,4-benzoquinone (DCBQ), and tetrachloro-1,4-benzoquinone (TCBQ) were measured in dry DCE by cyclic voltammetry at a 25 μm diameter platinum microelectrode. The formal redox potentials on the SHE scale were estimated by following the method described elsewhere.[15]

The initial stages of the photoexcitation of the porphyrin complex were studied by ultrafast transient absorption of the S_1 state. Two noncollinear optical parametric amplifiers (OPA) were pumped by the output of the femtosecond laser source (Clark-MXR CPA 2001). The OPAs were tuned for the pump beam at 560 nm and for the probe beam at 510 nm, producing 50 fs pulses at a repetition rate of 1 kHz and an average energy of 6 μJ. The pump and probe pulses were overlapped in the sample using a parabolic mirror. The probe beam was chopped at 210 Hz, and the signal intensity was measured by a photodiode connected to a lock-in amplifier (Stanford Research System SR830). Samples were placed in 1 mm thick glass cells mounted on a periodically moving translation stage.

3. Results and Discussion

3.1. Ultrafast Formation of the Charge-Separated State in the ZnTPPS−ZnTMPyP Ion Pair. As reported in previous publications, the anionic ZnTPPS and cationic ZnTMPyP form strong ion pairs in solution with an association constant of the order of 10^7 mol^{-1} dm^3.[15,19,20] Employing the Bjerrum model, we have estimated a center-to-center distance between both porphyrins of the order of 5.6 Å. The absorption spectra illustrated in Figure 2 reveal that the Soret and Q-bands of the ZnTPPS−ZnTMPyP ion pair are not a linear combination of the bands of the isolated porphyrins. Indeed, the absorption bands of the ion pair are broadened and red-shifted in comparison to the bands for the single porphyrins. These spectral features confirm the formation of Frenkel-type excitons as a

(5) Apostolakis, J.; Muegge, I.; Ermler, U.; Fritzsch, G.; Knapp, E. W. *J. Am. Chem. Soc.* **1996**, *118*, 3743.
(6) Chamber, J. Q. In *The Chemistry of Quinonoid Compounds*; Patai, S., Rappoport, Z., Eds.; John Wiley & Sons Ltd.: New York, 1988; pp 719−751.
(7) Bailey, I.; Ritchie, I. M.; Hewgill, F. R. *J. Chem. Soc., Perkin Trans. 2* **1983**, 645.
(8) Laviron, E. *J. Electroanal. Chem.* **1984**, *164*, 213.
(9) O'Malley, P. J. *Chem. Phys. Lett.* **1997**, *274*, 251−254.
(10) Gupta, N.; Linschitz, H. *J. Am. Chem. Soc.* **1997**, *119*, 6384−6391.
(11) Kim, J.; Chung, T. D.; Kim, H. *J. Electroanal. Chem.* **2001**, *499*, 78−84.
(12) Kim, H. S.; Chung, T. D.; Kim, H. *J. Electroanal. Chem.* **2001**, *498*, 209−215.
(13) Lahtinen, R.; Fermín, D. J.; Kontturi, K.; Girault, H. H. *J. Electroanal. Chem.* **2000**, *483*, 81−87.
(14) Ding, Z.; Quinn, B.; Bard, A. J. *J. Phys. Chem. B* **2001**, *105*, 6367−6374.
(15) Eugster, N.; Fermín, D. J.; Girault, H. H. *J. Phys. Chem. B* **2002**, 3428−3434.
(16) Fermín, D. J.; Ding, Z.; Duong, H. D.; Brevet, P. F.; Girault, H. H. *J. Phys. Chem. B* **1998**, *102*, 10334−10341.
(17) Fermín, D. J.; Ding, Z.; Duong, H. D.; Brevet, P. F.; Girault, H. H. *Chem. Commun.* **1998**, 1125−1126.
(18) Fermín, D. J.; Duong, H. D.; Ding, Z.; Brevet, P. F.; Girault, H. H. *Phys. Chem. Chem. Phys.* **1999**, *1*, 1461−1467.
(19) Fermín, D. J.; Duong, H. D.; Ding, Z.; Brevet, P. F.; Girault, H. H. *Electrochem. Commun.* **1999**, *1*, 29−32.
(20) Fermín, D. J.; Duong, H. D.; Ding, Z.; Brevet, P. F.; Girault, H. H. *J. Am. Chem. Soc.* **1999**, *121*, 10203−10210.
(21) Jensen, H.; Kakkassery, J. J.; Nagatani, H.; Fermín, D. J.; Girault, H. H. *J. Am. Chem. Soc.* **2000**, *122*, 10943−10948.

(22) See the web site dcwww.epfl.ch for a comprehensive list of free energy of ion transfer at various liquid|liquid interfaces.

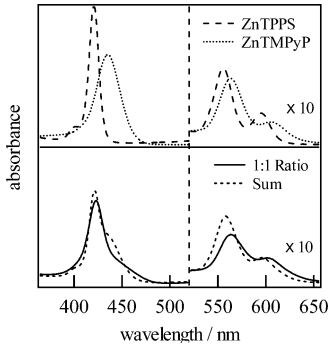

Figure 2. UV−visible absorption spectra of ZnTMPyP, ZnTPPS, and a 1:1 ratio of the two porphyrins in water. The dashed curve in the lower graphs corresponds to the sum of the absorption spectra of the isolated porphyrins. It can be clearly observed that the absorption spectrum of the ion pair is different from the sum of the spectra of both porphyrins.

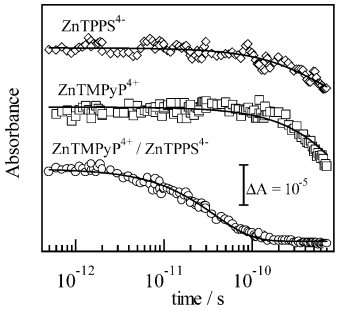

Figure 3. Femtosecond transient absorption of ZnTMPyP, ZnTPPS, and a 1:1 ratio of the two porphyrins in water. Solid lines correspond to exponential fittings with time constants equal to 1.6 and 0.6 ns for ZnTMPyP and ZnTPPS respectively, and 40 ps for the ion pair. The total concentration of porphyrins was 10^{-4} mol dm^{-3} in all cases.

result of the face-to-face conformation of the ion pair.[20,23,24] Recent Raman studies by Chen et al. revealed that CuTTPS and CuTMPyP undergo very slight structural changes of the porphyrin skeleton upon ion-pairing.[25]

The transient absorption responses shown in Figure 3 were obtained by pumping the porphyrins at 560 nm and probing at 510 nm. The relaxation observed in the case of single porphyrins corresponds to the depopulation of the S_1 state via radiative (fluorescence) and nonradiative (intersystem crossing) processes. The depopulation of the S_1 state for ZnTPPS and ZnTMPyP exhibits time constants of 1.6 and 0.6 ns, respectively. These values are within the range typically observed for the relaxation of the S_1 state of zinc tetraphenylporphyrins.[26−28] For an equimolar solution of both porphyrins, the decay of the excited state occurs within 40 ps and no response was observed for the triplet state between 400 and 700 nm at longer times. Considering that the driving force for electron transfer from ZnTMPyP to ZnTPPS is 0.31 eV, excluding the electrostatic energies associated with the charge of the molecules, it is expected that the excitation of the ion pair leads to the formation of an

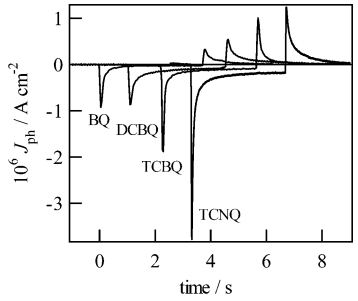

Figure 4. Photocurrent transient responses obtained in the presence of 10^{-3} mol dm^{-3} of 1,4-benzoquinone (BQ), 2,6-dichloro-1,4-benzoquinone (DCBQ), tetrachloro-1,4-benzoquinone (TCBQ), and tetracyanoquinodimethane (TCNQ) at $\Delta_o^w\phi = -0.12$ V. The photon flux at 477 nm was 7.6×10^{16} cm^{-2} s^{-1}.

intermolecular charge transfer state of the form

$$[(ZnTPPS^{4-})(ZnTMPyP^{4+})]^* \xrightarrow{k_q} [(ZnTPPS^{3-})(ZnTMPyP^{3+})]^{cs} \quad (1)$$

The charge-separated state generated by intermolecular quenching of the porphyrin ion pair plays a key role in the heterogeneous photoinduced electron-transfer processes across the liquid|liquid junction. As described in the next section, the phenomenological model employed for the analysis of the photocurrent responses is based on the competition between the heterogeneous electron transfer and the relaxation of the system to the ion-pair ground state. As this competition is dependent on the Galvani-potential difference and redox potential of the species in the organic phase, it is expected that the rates of relaxation and electron transfer are comparable.[20] Transition-state theory indicates that heterogeneous electron transfer across the liquid|liquid boundary takes place in the microsecond time scale.[15] Consequently, the lifetime of the charge-separated state generated by step (1) should extend into the microsecond time domain. The long living charge-separated state suggests that the kinetics of the back electron transfer step fall in the inverted Marcus region. Indeed, the thermodynamic driving force for the back reaction is well above 1 eV, which is considerably larger than the corresponding reorganization energy.[26,29] We shall come back to this point in the concluding sections of the paper.

3.2. Photocurrent Responses Originating from the Heterogeneous Photoreduction of Quinone Species. Photoexcitation of the ZnTPPS−ZnTMPyP complex adsorbed at the water|DCE interface in the presence of hydrophobic electron acceptors leads to photocurrent responses as illustrated in Figure 4. These photoresponses are associated with the heterogeneous electron transfer from the charge-separated state of the porphyrin ion pair to the electron acceptor in the organic phase. By contrast to the positive photocurrent measured in photoinduced oxidation processes,[15] electron injection into species in the organic phase yields negative photocurrents. Several features can be highlighted from the photocurrent transients in Figure 4: (i) The magnitude of the photocurrent is affected by the redox potential of the electron acceptor. (ii) the initial photoresponse is followed by a fast relaxation and an overshoot in the off-transient. The first point is related to the dependence of the electron-transfer

(23) Ojadi, E.; Selzer, R.; Linschitz, H. *J. Am. Chem. Soc.* **1985**, *107*, 7783−7784.
(24) Hugerat, M.; Levanon, H.; Ojadi, E.; Biczok, L.; Linschitz, H. *Chem. Phys. Lett.* **1991**, *181*, 400−406.
(25) Chen, D.-M.; Zhang, Y.-H.; He, T.-J.; Liu, F.-C. *Spectrochim. Acta, Part A* **2002**, *58*, 2291−2297.
(26) Kalyanasundaram, K. *Photochemistry of Polypyridine and Porphyrin Complexes*; Academic Press: London, 1992.
(27) Rodriguez, J.; Kirmaier, C.; Holten, D. *J. Am. Chem. Soc.* **1989**, *111*, 6500−6506.
(28) Yu, H.-Z.; Baskin, S.; Zewail, A. H. *J. Phys. Chem. A* **2002**, *106*, 9845−9854.
(29) Kalyanasundaram, K.; Neumannspallart, M. *J. Phys. Chem.* **1982**, *86*, 5163−5169.

rate constant on the thermodynamic driving force, which will be discussed in more detail in the next section. To extract the dynamics of photoinduced electron transfer, we shall first deconvolute the contributions from the relaxation phenomena as well as the double layer charging effects at short time scale.

The photocurrent transients in the presence of quinone species exhibit a biexponential decay, suggesting that two charge-transfer reactions generating positive currents are involved in the processes. In the case of TCNQ, the initial photocurrent exhibits a linear dependence on the light intensity, suggesting that the relaxation phenomena are not related to depletion of either the photoactive species or the electron acceptor at the interface. On the other hand, a substantial part of the photocurrent relaxation appears to be connected to back electron transfer from the reduced species to the oxidized porphyrin complex. Clear evidence for this is illustrated in Figure 5, where the time constant for the photocurrent decay during the photoreduction of TCBQ is decreased upon addition of the redox couple hexacyanoferrate(II)/(III) to the aqueous phase. In this case, the hexacyanoferrate can play the role of either supersensitizer or cosensitizer, depending on whether this redox couple reduces the oxidized ion-pair complex or the charge-separated state.[13] Previous studies of the photoreduction of TCNQ by the porphyrin ion pair have shown that the back electron transfer can be significantly diminished in the presence of an aqueous redox couple.[19]

In the case of electron acceptors such as benzoquinone, the photocurrent relaxation can also be associated with the possibility of interfacial protonation of the radical anion. Indeed, preliminary studies have shown that although the overall photocurrent slightly increases upon addition of hexacyanoferrate(II)/(III), the steady state value remains effectively zero.[13] Figure 5 clearly shows that, for a concentration of 5 10^{-4} mol dm^{-3} of the hexacyanoferrate couple, the effect on the photocurrent relaxation is relatively small in comparison to TCBQ. Assuming that the two relaxation phenomena are associated with the back electron transfer and interfacial protonation of the quinones, the photoreduction process can be described in terms of the following elementary steps,

ultrafast interporphyrin charge separation:

$$S_w \xrightarrow{h\nu} S_w^* \xrightarrow{k_q} S_w^{cs} \quad (2)$$

charge-separated state recombination: $S_w^{cs} \xrightarrow{k_d} S_w$ (3)

heterogeneous electron transfer:

$$S_w^{cs} + Q_o \xrightarrow{k_{et}} [S_w^+ \cdots Q_o^{\bullet -}] \quad (4)$$

back electron transfer: $[S_w^+ \cdots Q_o^{\bullet -}] \xrightarrow{k_b} S_w + Q_o$ (5)

separation of photoproducts: $[S_w^+ \cdots Q_o^{\bullet -}] \xrightarrow{k_{ps}} S_w^+ + Q_o^{\bullet -}$ (6)

interfacial protonation: $Q_o^{\bullet -} + H_w^+ \xrightarrow{k_{tr}} QH_o$ (7)

where S_w^* corresponds to the photoexcited ion pair and S_w^{cs} to the charge-separated state as indicated in eq 1. The generation of the intermediate species $[S_w^+ \cdots Q_o^{\bullet -}]$ in step (4) involves the heterogeneous electron transfer responsible for the negative photocurrent. The photocurrent relaxation is determined by the competition between the back electron transfer (5) and the separation of photoproducts (step (6)). In the case of interfacial protonation, step (7) is also in competition with the diffusion of the semiquinone away from the interface. The flux of charges across the liquid|liquid boundary is balanced by mass transport phenomena involving the redox species in the organic phase and the regeneration of the ground state of the ion pair at the interface.

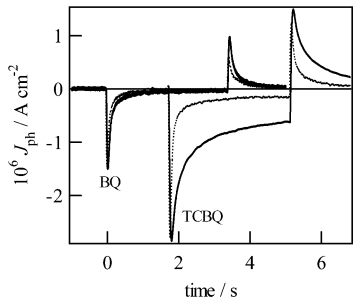

Figure 5. Photocurrent transient responses obtained in the presence of 10^{-3} mol dm^{-3} of BQ and TCBQ at $\Delta_o^w\phi = -0.12$ V, in the absence (gray lines) and in the presence (black lines) of 5×10^{-4} M hexacyanoferrate(II). The photon flux at 477 nm was 7.6×10^{16} cm^{-2} s^{-1}.

To solve the differential equations associated with the set of elementary reactions, we shall consider that the concentrations of the electron acceptor and protons at the interface remain constant. Taking into account that the competition between steps (3) and (4) takes place several orders of magnitude faster than the subsequent steps,[15] we can assume a steady-state concentration of the charge-separated ion pair at the interface. Given the fast interporphyrin electron transfer, the concentration of the charge-separated state ($[S^{cs}]$) is directly related to the flux of photons across the interface:

$$[S^{cs}] = \frac{I_0 \sigma_S}{k_{et} + k_d} \Gamma_S \quad (8)$$

Here I_0, σ_S, and Γ_S correspond to the photon flux across the interface, the light capture cross section, and the concentration of the adsorbed porphyrin ion pair in the ground state. The electron-transfer rate constant k_{et} is expressed as a pseudo-first-order rate constant with respect to the sensitizer, i.e., $k_{et} = k_{et}^{II}[Q_o]$. The differential equations involving the concentrations of the intermediate species ([SQ]) and the semiquinone radical ($[Q_o^{\bullet -}]$) are given by

$$\frac{d[SQ]}{dt} = g - (k_b + k_{ps})[SQ] \quad (9)$$

$$\frac{d[Q^{\bullet -}]}{dt} = k_{ps}[SQ] - (k_{tr} + k_{di})[Q^{\bullet -}] \quad (10)$$

In this treatment, we have expressed the disappearance of the semiquinone radical from the interface as a first-order process (k_{di}) to simplify the analysis. A more rigorous treatment involves the computing of the concentration profiles of the products. Considering that the steady-state photocurrents are rather small under the experimental conditions, this approximation has very little effect on the present analysis of the photocurrent transients. The parameter g in eq 9 corresponds to the flux of electron injection from the charge-separated state,

$$g = k_{et}[S^{cs}] = \frac{k_{et} I_0 \sigma_S}{k_{et} + k_d} \Gamma_S \tag{11}$$

To obtain an expression for the photocurrent as a function of time, the concentrations of the intermediate and product species are transformed in the Laplace plane yielding

$$\overline{[SQ]} = \frac{g}{s}\left(\frac{1}{s + k_b + k_{ps}}\right) \tag{12}$$

$$\overline{[Q^{\bullet -}]} = \frac{g}{s}\left(\frac{k_{ps}}{s + k_b + k_{ps}}\right)\left(\frac{1}{s + k_{tr} + k_{di}}\right) \tag{13}$$

where s is the Laplace variable. The photocurrent response involves contributions from all the steps featuring charge transfer across the liquid|liquid boundary, i.e., steps (4), (5), and (7). Consequently, it follows

$$J_{ph} = -F(k_{et}[S^{cs}] - k_b[SQ] - k_{tr}[Q^{\bullet -}]) \tag{14}$$

which can be expressed in the Laplace plane as

$$\overline{J_{ph}} = -F(k_{et}\overline{[S^{cs}]} - k_b\overline{[SQ]} - k_{tr}\overline{[Q^{\bullet -}]}) \tag{15}$$

It should also be considered that the photocurrent responses are attenuated by the *RC* component of the cell at short times. This parameter can be introduced into expression (15) yielding[18,30]

$$\overline{J_{ph}} = -F(k_{et}\overline{[S^{cs}]} - k_b\overline{[SQ]} - k_{tr}\overline{[Q^{\bullet -}]})\left(\frac{1}{1 + RCs}\right) \tag{16}$$

The inverse Laplace transform of eq 16 provides the following relation for the photocurrent as a function of time under constant illumination:

$$J_{ph} = -Fg(\alpha - \beta - \gamma) \tag{17}$$

where

$$\alpha = 1 - \exp\left(-\frac{t}{RC}\right) \tag{18}$$

$$\beta = k_b\left(\frac{1 - \exp(-(k_b + k_{ps})t)}{k_b + k_{ps}} - RC\frac{\exp(-(k_b + k_{ps})t) - \exp(-t/RC)}{1 - RC(k_b + k_{ps})}\right) \tag{19}$$

$$\gamma = \frac{k_{ps}k_{tr}}{k_b + k_{ps} - k_{tr} - k_{di}}\left(\frac{1 - \exp(-(k_b + k_{ps})t)}{k_b + k_{ps}} - \frac{1 - \exp(-(k_{tr} + k_{di})t)}{k_{tr} + k_{di}} - RC\frac{\exp(-(k_b + k_{ps})t) - \exp(-t/RC)}{1 - RC(k_b + k_{ps})} + RC\frac{\exp(-(k_{tr} + k_{di})t) - \exp(-t/RC)}{1 - RC(k_{tr} + k_{di})}\right) \tag{20}$$

The term α is associated with the initial rise of the photocurrent response determined by the *RC* constant of the cell. As the resistance between the two reference electrodes tends to zero, this parameter approaches unity; i.e., the photocurrent rise will be in-phase with the light excitation. The effect of the *RC* constant is illustrated in Figure 6a. The terms β and γ describe the exponential decays associated with the back electron transfer (5) and the heterogeneous protonation (7), respectively. In Figure 6b, the transient evolution of the parameters α, β, and γ are contrasted to the photocurrent as estimated from eq 17, taking the *RC* constant as 30 ms. This figure clearly indicates that to estimate the flux of electron injection g from the photocurrent response, the contributions from the fast relaxation processes and the *RC* constant should be deconvoluted. Fitting of eq 17 to photocurrent transients for the various electron acceptors and Galvani potential differences provides consistent values for g, k_{ps}, k_b, k_{tr}, and k_{di}. A typical fitting of the photocurrent transients is exemplified in Figure 6c. Initial values for *RC* were estimated from impedance measurements. Values of k_b were obtained in the range $10-50$ s^{-1}, while k_{tr} was of the order of $1-5$ s^{-1}. These estimations are consistent with independent studies based on intensity modulated photocurrent spectroscopy, which will be discussed in a subsequent paper. The key parameter that we shall analyze in the next section is g, which contains information

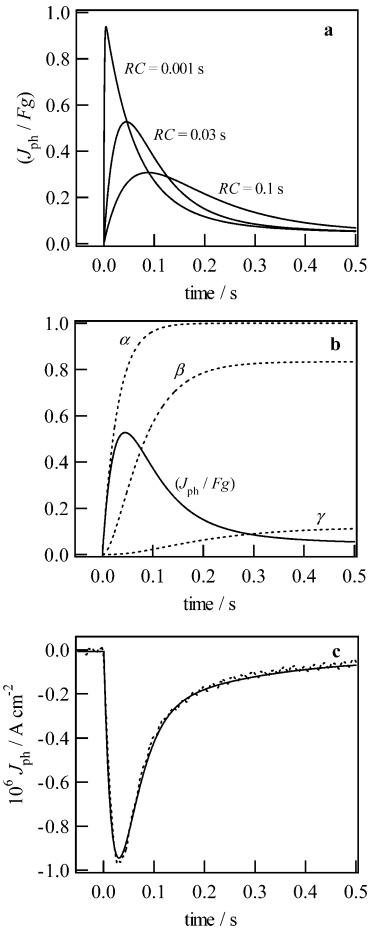

Figure 6. Effect of the *RC* constant of the cell on the photocurrent responses as evaluated from eq 17, employing $k_b = 15$ s^{-1}, $k_{ps} = 3$ s^{-1}, $k_{tr} = 5$ s^{-1}, and $k_{di} = 2$ s^{-1} (a). Photocurrent response and corresponding α, β, and γ terms as evaluated from eqs 17−20 for a *RC* constant of 0.03 s (b). Photocurrent response obtained in the presence of 10^{-3} mol dm^{-3} of BQ at $\Delta_o^w\phi = -0.12$ V (dashed line) and numerical evaluation of eq 17 (solid line) employing $k_b = 32$ s^{-1}, $k_{ps} = 4.7$ s^{-1}, $k_{tr} = 4.1$ s^{-1}, $k_{di} = 0.4$ s^{-1}, *RC* = 0.025 s, and $g = 2.2 \times 10^{-11}$ mol s^{-1} cm^{-2} (c).

(30) Peter, L. M. *Chem. Rev.* **1990**, *90*, 753−769.

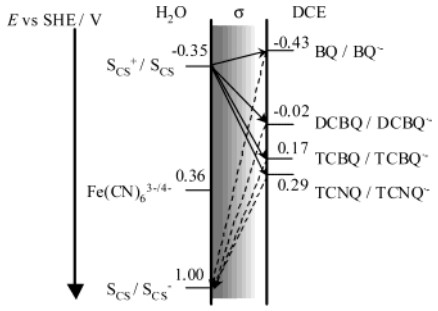

Figure 7. Formal redox potentials of the ZnTMPyP porphyrin and electron acceptors in the organic phase vs SHE. The liquid|liquid boundary is denoted σ. Solid arrows are associated with the forward electron transfer from the porphyrins to the quinones, while dashed arrows represent the back electron transfer process as described in eq 5.

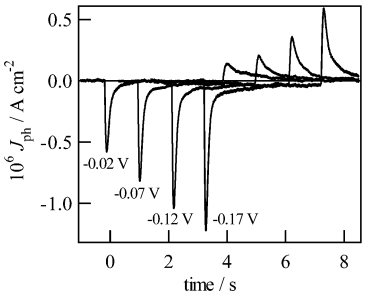

Figure 8. Photocurrent transient responses obtained in the presence of 10^{-3} mol dm^{-3} TCBQ at various Galvani potential differences. The photon flux at 477 nm was 7.6×10^{16} cm^{-2} s^{-1}.

of the rate of photoinduced heterogeneous electron transfer (eq 11).

3.3. Flux of Heterogeneous Electron Injection as a Function of the Thermodynamic Driving Force. As mentioned in the previous section, the magnitude of the photocurrent responses exemplified in Figure 4 shows a clear dependence on the redox potential of the electron acceptor. This behavior can be qualitatively rationalized by the diagram depicted in Figure 7, where the redox potential of the electron acceptor in bulk DCE are contrasted with that of the reduced ZnTMPyP in water.[26] Although the energy levels of the porphyrins are affected to a certain extent by the excitonic coupling, it can be taken as a first approximation that the reduced ZnTMPyP and the oxidized ZnTPPS moieties determine the redox potentials of the complex. Consequently, the formal Gibbs free energy for the heterogeneous electron transfer ($\Delta G_{et}^{o\prime}$) can be expressed as

$$\Delta G_{et}^{o\prime} = F([E_{Scs/S^+}^{o\prime,w}]_{SHE} - [E_{Q/Q\bullet^-}^{o\prime,DCE}]_{SHE} + \Delta_o^w\phi) \quad (21)$$

where the values of $[E_{Scs/S+}^{o\prime,w}]_{SHE}$ and $[E_{Q/Q\bullet-}^{o\prime,DCE}]_{SHE}$ are as indicated in Figure 7 and $\Delta_o^w\phi$ is the Galvani potential difference across the water|DCE interface. A rather surprising behavior is observed in the presence of BQ, where photocurrent responses are observed even if the apparent $\Delta G_{et}^{o\prime}$ is positive. As discussed later, this intriguing result can be rationalized in terms of changes in the apparent redox potential of BQ at the liquid|liquid boundary.

According to eq 21, the magnitude of the photocurrent for a given electron acceptor increases as $\Delta_o^w\phi$ is shifted toward more negative values. This behavior is exemplified in Figure 8 for the case of TCBQ. A similar potential dependence of the photocurrent was qualitatively observed for all the electron acceptors. From eqs 11 and 17, the sharp increase in the photocurrent magnitude can be rationalized in terms of an increase of the driving force for the heterogeneous electron transfer. Our previous studies have shown that the surface concentration of the ion-pair complex at the water|DCE interface is effectively independent of $\Delta_o^w\phi$.[13,15,20] Consequently, extracting the parameter g from photocurrent transients at various potentials and for the different electron acceptors provides information on the dependence of k_{et} on $\Delta G_{et}^{o\prime}$.[15]

Assuming that the redox centers are separated by an average distance d_{cc} and a step change in the dielectric properties of the electrolytes, the bimolecular electron-transfer rate constant can be expressed as

$$k_{et}^{II} = 2\pi\kappa\nu(a_S + a_Q)\Delta R^3 \exp(-\Delta G_{act}/k_BT) \quad (22)$$

where κ is the Landau−Zener transmission coefficient, ν is the frequency of nuclear motion, and ΔR is the characteristic distance where the volume integrand is maximized.[31−34] The parameters a_S and a_Q correspond to the molecular radii of the sensitizer and the redox quencher. If the work terms for approaching reactants and separating products are neglected, the activation energy is given by

$$\Delta G_{act} = \frac{(\lambda + \Delta G_{et}^{o\prime})^2}{4\lambda} \quad (23)$$

where λ is the reorganization energy involving contributions from internal conformation changes of the reactants as well as the solvation structure during the electron-transfer step. With rearrangement of eqs 11, 22, and 23, the flux of electron injection g can be expressed as

$$g = I_0\sigma\Gamma_S \frac{\exp(-(\lambda + \Delta G_{et}^{o\prime})^2/4\lambda k_BT)}{\exp(-(\lambda + \Delta G_{et}^{o\prime})^2/4\lambda k_BT) + k_d/Z} \quad (24)$$

where the parameter Z corresponds to the activationless limit of the electron-transfer rate constant in units of the homogeneous pseudo first-order rate constant with respect to S_w^{cs}; i.e.

$$Z = 2\pi\kappa\nu(a_S + a_Q)\Delta R^3[Q_o]/d_{cc} \quad (25)$$

The flux of electron injection obtained from fittings of the photocurrent transients is plotted in Figure 9. The dashed line in this figure shows the theoretical values of g, as calculated from eq 24. The parameters λ and k_d/Z were 1.05 eV and 0.5 as extracted from our previous kinetics studies of the photooxidation of ferrocene derivatives under identical conditions.[15] The good agreement between predicted and experimental fluxes of electron injection for TCNQ, TCBQ, and DCBQ indicates that the dynamics of electron transfer involving these redox species as well as ferrocene derivatives is controlled by a single λ value. As discussed previously, λ has a major contribution from the solvent reorganization part, which is determined by the distance separating the redox centers, i.e., d_{cc}.[15] The magnitudes of the bimolecular electron-transfer rate constants

(31) Marcus, R. A. *J. Phys. Chem.* **1990**, *94*, 4152−4155.
(32) Marcus, R. A. *J. Phys. Chem.* **1990**, *94*, 1050−1055.
(33) Marcus, R. A. *J. Phys. Chem.* **1991**, *95*, 2010−2013.
(34) Smith, B. B.; Halley, J. W.; Nozik, A. J. *Chem. Phys.* **1996**, *205*, 245−67.

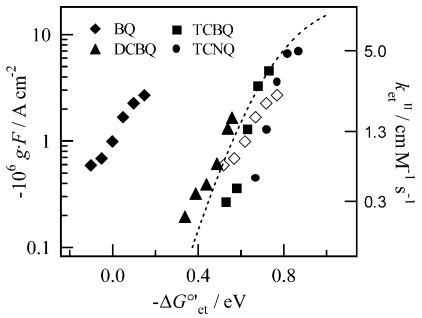

Figure 9. Flux of electron injection and bimolecular interfacial electron-transfer rate constant as a function of the Gibbs energy of electron transfer. The rate constant was estimated assuming a value for $d_{cc} = 1$ nm. The dashed line corresponds to the flux of electron injection as calculated from eq 24, taking λ and k_d/Z as 1.05 eV and 0.5, respectively. The photon flux I_0, light capture cross section σ at 477 nm, and excess concentration Γ_s were taken as 7.6×10^{16} cm^{-2} s^{-1}, 10^{-17}cm^2, and 2.5×10^{14} cm^{-2}, respectively.

estimated from the fluxes of electron injection are also shown in Figure 9, taking $d_{cc} = 1$ nm.

3.4. Apparent Redox Potential of BQ at the Liquid|liquid Boundary: Proton Transfer vs Hydrogen Bonding. One of the most striking results in Figure 9 is the apparent uphill heterogeneous electron injection to BQ. The behavior observed for BQ clearly falls outside the trend observed for the other electron acceptors. To rationalize these results, it can be proposed that the redox properties of BQ at the liquid|liquid boundary are significantly different from those observed in bulk DCE. Effectively, the $\Delta G_{et}{}^{o\prime}$ is estimated from eq 21 taking the formal redox potential as the half-wave reduction potential of BQ on a Pt microelectrode in a dry DCE solution. The hollow diamonds in Figure 9 are obtained by shifting this redox potential by ca. 0.6 V toward more positive values. In principle, substantial displacement of the reduction potential of BQ can take place via the formation of H-bonds as well as interfacial protonation processes. These effects are expected to be less significant for DCBQ and TCBQ. The point that we shall address here is whether this apparent shift is either related to H-bonding or to the semiquinone protonation.

As indicated in eq 14, the protonation step involves the transfer of a net positive charge from water to DCE, which manifest itself as a positive current response. If the proton-transfer step occurs at time scales shorted than the relaxation associated with the *RC* component of the cell, the charge transfer originating from the quinone reduction is effectively counter-balanced and no net photocurrent can be measured under potentiostatic conditions. However, analysis of the photocurrent relaxation as illustrated in Figure 6c clearly shows that the proton transfer occurs in the subsecond time domain, i.e., over 4 orders of magnitude slower than the electron-transfer step to BQ. Consequently, the protonation equilibrium cannot be invoked as the origin of the positive shift of the effective reduction potential of BQ as estimated from the flux of electron injection from the charge-separated intermediate state.

Nonetheless, it appears somewhat surprising that shifts of the order of 0.6 V of the reduction potential can be induced by the formation of interfacial H-bonds. For instance, Kim et al. have reported changes of approximately 200 mV in the reduction potential of BQ in acetonitrile in the presence of $NH_4{}^+$.[11] However, theoretical estimations of the electron affinity for BQ hydrogen bonded to four water molecules predicted increments of the order of 1.1 eV.[9] We have also extended our studies to other quinones such as tetramethylquinone, which redox potential exhibits a stronger dependence on hydrogen bonding. However, the redox potential of this quinone is significantly more negative than for BQ and no effective electron injection was observed within the polarizable window.

4. Conclusions

Ultrafast time-resolved spectroscopy and dynamic photoelectrochemical measurements have provided a detailed picture of the initial stages in the photoreduction of quinone species by porphyrin ion pairs assembled at the water|DCE. Femtosecond transient absorption shows that the ZnTPPS−ZnTMPyP ion pair undergoes a quenching process in 40 ps, involving the thermally equilibrated S_1 state. On thermodynamic grounds, this reaction can be associated with an electron injection from the ZnTPPS to ZnTMPyP, generating a charge-separated state that is subsequently involved in the heterogeneous photoelectrochemical processes. The electron-transfer reaction from the charge-separated state to the acceptors in the organic phase takes place in the microsecond time scale. This reaction sequence resembles the mechanism elucidated for the photocurrent responses at liquid|liquid interfaces in the presence of dye-sensitized colloidal TiO_2 particles.[35] The strong electronic coupling between the dye and the metal oxide leads to charge injection in the femtosecond time scale.[36] Nevertheless, the lifetime of the charge-separated state extends into the microsecond regime,[37,38] allowing heterogeneous electron transfer to take place across the liquid|liquid boundary.[35] As concluded for the dye-sensitized TiO_2 system, we strongly believe that the slow recombination in the charge-separated state of the porphyrin ion pair is a manifestation of the inverted region for the electron transfer.

The heterogeneous electron transfer involving the charge-separated state and the electron acceptors in the organic phase manifests itself by negative photocurrents under potentiostatic conditions. The photocurrent transients in the presence of quinones exhibit a strong relaxation connected to back electron transfer reaction and interfacial protonation of the semiquinone radical in the range 0.02−1 s. The flux of electron injection shows a clear dependence on the Gibbs free energy of electron transfer. The behavior observed for TCNQ, DCBQ, and TCBQ could be rationalized in terms of the Marcus limit for nonadiabatic electron transfer featuring solvent reorganization energies of the order of 1 eV. The results obtained for these electron acceptors appear entirely consistent with our previous studies on photooxidation of ferrocene derivatives, confirming that the dynamics of charge transfer are fundamentally determined by the characteristic the distance separating the redox centers.[15] This distance is comparable to the density profiles of each solvent or the "intermixing region" at the liquid|liquid junction.[39−42]

(35) Fermín, D. J.; Jensen, H.; Moser, J. E.; Girault, H. H. *ChemPhysChem.* **2003**, *4*, 85−89.
(36) Huber, R.; Moser, J. E.; Gratzel, M.; Wachtveitl, J. *J. Phys. Chem. B* **2002**, *106*, 6494−6499.
(37) Moser, J. E.; Gratzel, M. *Chem. Phys.* **1993**, *176*, 493−500.
(38) Huber, R.; Sporlein, S.; Moser, J. E.; Gratzel, M.; Wachtveitl, J. *J. Phys. Chem. B* **2000**, *104*, 8995−9003.
(39) Benjamin, I. *Annu. Rev. Phys. Chem.* **1997**, *48*, 407.
(40) Benjamin, I. *Chem. Rev.* **1996**, *96*, 1449−1475.
(41) Strutwolf, J.; Barker, A. L.; Gonsalves, M.; Caruana, D. J.; Unwin, P. R.; Williams, D. E.; Webster, J. R. P. *J. Electroanal. Chem.* **2000**, *483*, 163−173.

Scheme 2. Schematic Diagram of the Early Stages of the Heterogeneous Photoreduction of BQ by the ZnTPPS−ZnTMPyP Ion Pair at the Water|1,2-Dichloroethane Interface

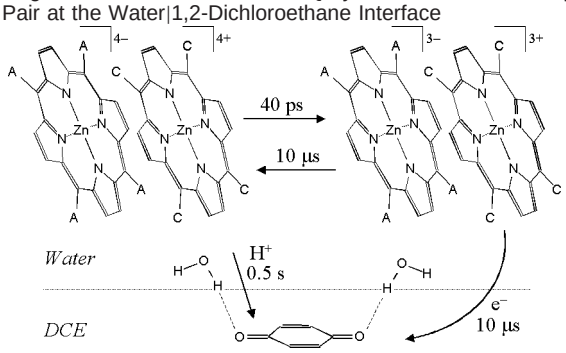

Finally, the dynamics of BQ photoreduction was rather different from the one observed for the other electron acceptors. The analysis appears to show that the effective redox potential of BQ at the liquid|liquid boundary is approximately 0.6 V more positive than in bulk DCE. This change in the redox potential can be rationalized in terms of the predicted increase of the electron affinity of BQ via the formation of hydrogen bonds.[9] This analysis reveals a strong specific interaction of BQ at the interfacial boundary between two immiscible liquids, which can shed more light on the electrochemical reactivity of naturally occurring quinones in biological membranes. The early stages of the BQ photoreduction can be summarized in Scheme 2. A loose comparison between Schemes 1 and 2 reveals some similarities between the mechanisms highlighted here and the one found in the reaction center of purple bacteria. Both processes are initiated by an ultrafast photoinduced charge separation that is followed by electron injection into quinone molecules. The interfacial proton transfer step occurs at a significantly longer time scale. In subsequent publications, we shall deal with the photocurrent relaxation dynamics in more detail, in particular the apparently slow proton transfer to the reduced semiquinone.

Acknowledgment. This work has been sponsored by the Fonds National Suisse de la Recherche Scientifique (Projects 2000-55692.98 and 2000-067050.01). We are grateful to Dr. Jacques E. Moser and Dr. Serge Pellet from the Laboratorie de Photoniques et Interfaces for their valuable support in the ultrafast time-resolved studies. We also acknowledge the technical support by Valerie Devaud. The Laboratoire d'Electrochimie Physique et Analytique is part of the European TMR network SUSANA (Supramolecular Self-Assembly of Interfacial Nanostructures).

JA029589N

(42) Webster, R. D.; Beaglehole, D. *Phys. Chem. Chem. Phys.* **2000**, *2*, 5660−5666.